


Fraction of χ_c Decays in Prompt J/ψ Production Measured in $p\text{Pb}$ Collisions at $\sqrt{s_{\text{NN}}} = 8.16$ TeV

R. Aaij *et al.**
(LHCb Collaboration)

 (Received 2 November 2023; revised 5 January 2024; accepted 6 February 2024; published 8 March 2024)

The fraction of χ_{c1} and χ_{c2} decays in the prompt J/ψ yield, $F_{\chi_c \rightarrow J/\psi} = \sigma_{\chi_c \rightarrow J/\psi} / \sigma_{J/\psi}$, is measured by the LHCb detector in $p\text{Pb}$ collisions at $\sqrt{s_{\text{NN}}} = 8.16$ TeV. The study covers the forward ($1.5 < y^* < 4.0$) and backward ($-5.0 < y^* < -2.5$) rapidity regions, where y^* is the J/ψ rapidity in the nucleon-nucleon center-of-mass system. Forward and backward rapidity samples correspond to integrated luminosities of 13.6 ± 0.3 and 20.8 ± 0.5 nb $^{-1}$, respectively. The result is presented as a function of the J/ψ transverse momentum $p_{\text{T},J/\psi}$ in the range $1 < p_{\text{T},J/\psi} < 20$ GeV/ c . The $F_{\chi_c \rightarrow J/\psi}$ fraction at forward rapidity is compatible with the LHCb measurement performed in pp collisions at $\sqrt{s} = 7$ TeV, whereas the result at backward rapidity is 2.4σ larger than in the forward region for $1 < p_{\text{T},J/\psi} < 3$ GeV/ c . The increase of $F_{\chi_c \rightarrow J/\psi}$ at low $p_{\text{T},J/\psi}$ at backward rapidity is compatible with the suppression of the $\psi(2S)$ contribution to the prompt J/ψ yield. The lack of in-medium dissociation of χ_c states observed in this study sets an upper limit of 180 MeV on the free energy available in these $p\text{Pb}$ collisions to dissociate or inhibit charmonium state formation.

DOI: [10.1103/PhysRevLett.132.102302](https://doi.org/10.1103/PhysRevLett.132.102302)

Heavy ion collisions in the relativistic regime provide an opportunity to release quarks and gluons from hadrons and form a hot and dense quark-gluon plasma (QGP), the same state of matter theorized to exist microseconds after the big bang and to compose the core of neutron stars [1]. While there are many indications of QGP formation in nucleus-nucleus collisions at RHIC and the LHC, its formation in small systems such as proton-nucleus collisions is not firmly established. The observation of collective particle flow in $p\text{Pb}$ collisions at the LHC, and pA and dA collisions at RHIC, suggests the existence of QGP droplets in these collisions (see, for example, [2]), but a lack of other signatures prevents a conclusion. Quarkonium states have a broad range of binding energies [3] of the same order of magnitude as the freeze-out temperature, the minimum temperature needed to form a QGP [4–6]. The spectrum of quarkonium states that survive nucleus collisions is a powerful tool to determine the free energy and temperature reached by the initial stage of heavy ion collisions. However, a quarkonium state can also be broken by its interaction with comoving particles if the particle multiplicity is high enough, as observed in the nucleus-going direction in proton- and deuteron-nucleus collisions [7].

The nuclear modification factor, defined as the ratio between the particle yield per nucleon interaction measured in heavy ion and pp collisions, is the most commonly used observable to quantify nuclear effects. The spin-1 ground-state charmonium meson J/ψ , with a binding energy of 640 MeV, has a nuclear modification factor similar to the open charm meson D^0 at forward and backward rapidity ranges in $p\text{Pb}$ collisions [8]. This observation indicates that the nuclear modification factor observed in J/ψ yields in these collisions can be attributed solely to nuclear modification of parton densities before the formation of the $c\bar{c}$ pair. The charmonium state $\psi(2S)$, with a binding energy of 50 MeV, has a suppression stronger than the J/ψ state at backward rapidity in $p(d)A$ collisions at RHIC [9] and the LHC [10–12], indicating that this weakly bound state is also suppressed by final-state nuclear effects.

Additional constraints on the free local energy produced in pA collisions, which would dissociate or prevent charmonium state formation, can be provided by the χ_{c1} and χ_{c2} states. These have binding energies of 220 and 180 MeV, respectively. The P -wave charmonium states χ_{cn} are mainly reconstructed from the radiative decay $\chi_{cn} \rightarrow J/\psi\gamma$ with branching ratios 1.4%, 34%, and 19% for $n = 0, 1$, and 2 [13]. The production of χ_{c0} mesons is rarely studied in this decay mode, due to its small branching ratio. Measurements of χ_c production typically require high detection efficiency for low-energy photons, and effective discrimination against the overwhelming π^0 decay sources producing large combinatorial backgrounds in the $J/\psi\gamma$ mass distribution. For these reasons, χ_c measurements in

*Full author list given at the end of the article.

Published by the American Physical Society under the terms of the [Creative Commons Attribution 4.0 International license](https://creativecommons.org/licenses/by/4.0/). Further distribution of this work must maintain attribution to the author(s) and the published article's title, journal citation, and DOI. Funded by SCOAP³.

heavy ion collisions are rare. There are two χ_c measurements in nucleus collisions: (i) HERA-B measured the fraction of χ_c decays in J/ψ production in proton on C and W targets at $\sqrt{s_{\text{NN}}} = 41.6$ GeV [14], showing no dependence on the target material and (ii) PHENIX measured the $\chi_c/J/\psi$ fraction in $d\text{Au}$ collisions at $\sqrt{s_{\text{NN}}} = 200$ GeV [15], consistent with measurements in pp collisions at the same energy within the large statistical uncertainty. The identified χ_{c1} and χ_{c2} yields measured by the LHCb Collaboration in $p\text{Pb}$ collisions at $\sqrt{s_{\text{NN}}} = 8.16$ TeV are consistent [16], although with large uncertainties given the difficulty in resolving the mass peaks.

This Letter reports, for the first time at the LHC, the fraction $F_{\chi_c \rightarrow J/\psi}$ of $\chi_c \rightarrow (J/\psi \rightarrow \mu^+\mu^-)\gamma$ decays in prompt $J/\psi \rightarrow \mu^+\mu^-$ yields. The measurement is made in eight $p_{\text{T},J/\psi}$ ranges over $1 < p_{\text{T},J/\psi} < 20$ GeV/ c in $p\text{Pb}$ collisions at $\sqrt{s_{\text{NN}}} = 8.16$ TeV at forward ($1.5 < y^* < 4.0$) and backward ($-5.0 < y^* < -2.5$) rapidities, where y^* is the J/ψ rapidity in the nucleon-nucleon center-of-mass system. Prompt J/ψ mesons are produced directly when $c\bar{c}$ pairs form a bound state (direct production) or via decays of higher-mass charmonium states (feed-down contribution). The measured χ_c yield is the sum of the χ_{c1} and χ_{c2} yields, which minimizes the uncertainties related to the separation of these states. The fraction $F_{\chi_c \rightarrow J/\psi}$ is obtained by

$$F_{\chi_c \rightarrow J/\psi} \equiv \frac{\sigma_{\chi_c \rightarrow J/\psi\gamma}}{\sigma_{J/\psi}} = \frac{N_{\chi_c \rightarrow J/\psi\gamma}}{N_{J/\psi} \varepsilon_{\chi_c/J/\psi}}, \quad (1)$$

where $N_{\chi_c \rightarrow J/\psi\gamma}$ and $N_{J/\psi}$ are the prompt $\chi_c \rightarrow J/\psi\gamma$ and J/ψ yields, and $\varepsilon_{\chi_c/J/\psi}$ is the fraction of $\chi_c \rightarrow J/\psi\gamma$ decays which are detected in the LHCb acceptance relative to the decays where only the J/ψ is detected. The contribution from B hadron decays is negligible after the selection of prompt J/ψ decays.

The LHCb detector is a single-arm forward spectrometer described in Refs. [17,18]. The silicon-strip vertex detector (VELO) surrounding the interaction region allows the determination of the position of the collision point, the primary vertex (PV). Charged particle tracks are determined by the combination of hits in the VELO, a large-area silicon-strip detector located upstream of a dipole magnet with a bending power of about 4 Tm, and three stations of silicon-strip detectors and straw drift tubes (OT) placed downstream of the magnet. Muons are identified by a system composed of alternating layers of iron and multi-wire proportional chambers behind electromagnetic and hadronic calorimeters. Photons are identified by the calorimeter system [19] consisting of a scintillating pad detector (SPD), a preshower system (PS), an electromagnetic (ECAL) calorimeter, and a hadronic (HCAL) calorimeter. The SPD and PS are designed to discriminate between signals from photons and electrons, while the ECAL and HCAL provide the energy measurement and

identification of photons and neutral hadrons. The relative energy resolution of the ECAL is $8\%/\sqrt{E} + 0.9\%$, where E is in GeV.

This analysis is based on data acquired during the 2016 LHC heavy-ion run, where the LHCb experiment recorded proton and ^{208}Pb ion collisions at a center-of-mass energy per nucleon pair of $\sqrt{s_{\text{NN}}} = 8.16$ TeV. The forward (positive) rapidity sample is collected in collisions where the proton follows the direction from the VELO to the muon detectors, namely, $p\text{Pb}$ collisions, corresponding to an integrated luminosity of 13.6 ± 0.3 nb $^{-1}$. The backward (negative) rapidity sample is obtained with a reverse beam direction, $\text{Pb}p$ collisions, with 20.8 ± 0.5 nb $^{-1}$ integrated luminosity.

The on-line event selection used in this analysis is performed by a trigger system consisting of a hardware stage that selects events containing at least one muon candidate, and two software trigger stages in which events with two tracks identified as muons with $p_{\text{T}} > 500$ MeV/ c are selected. The muon pair is required to have an invariant mass within 150 MeV/ c^2 of the known J/ψ mass [13]. In the off-line selection, muons are identified by a neural network algorithm [18,20]. The muon also must satisfy the momentum requirements $p_{\text{T}} > 600$ MeV/ c , $p > 8$ GeV/ c , and be in the LHCb pseudorapidity range $2 < \eta < 5$. The J/ψ candidate is selected by requiring the muon pair invariant mass to be within 80 MeV/ c^2 of its known mass and its transverse momentum $p_{\text{T},J/\psi}$ must be larger than 1 GeV/ c . The J/ψ candidate must be consistent with originating from the collision point.

Photons are identified as isolated clusters in the ECAL. The cluster must not belong to a charged particle or a π^0 decay with 80% confidence level as determined by neural network algorithms. The photon must be in the ECAL acceptance $2 < \eta < 4.5$ and have transverse momentum $p_{\text{T},\gamma} > 400$ MeV/ c .

The detector performance for the J/ψ and χ_c signals are studied using simulated samples generated by PYTHIA [21] and embedded with events generated by EPOS [22], which accounts for the underlying event activity of $p\text{Pb}$ collisions. Decays of short-lived particles are performed with the EvtGen decay package [23]. Radiative QED corrections to the decays containing charged particles in the final state are applied with the PHOTOS package [24]. The generated χ_{c1} and χ_{c2} decays are required to have both muons from the J/ψ decay in the LHCb acceptance. The response of the LHCb detector is modelled using GEANT4 [25]. Weights are assigned to the simulated events such that the VELO cluster multiplicity matches that of the data. The LHCb detection efficiency correction $\varepsilon_{\chi_c/J/\psi}$ is obtained from the simulated χ_c sample using Eq. (1), where $F_{\chi_c \rightarrow J/\psi} = 1$ by definition.

The selected sample is overwhelmingly composed of combinatorial background (CBG). The remaining components are correlated background, also called physics background, and the signal χ_c decays. This analysis uses the invariant mass difference $\Delta M = M_{\mu^+\mu^-\gamma} - M_{\mu^+\mu^-}$ for

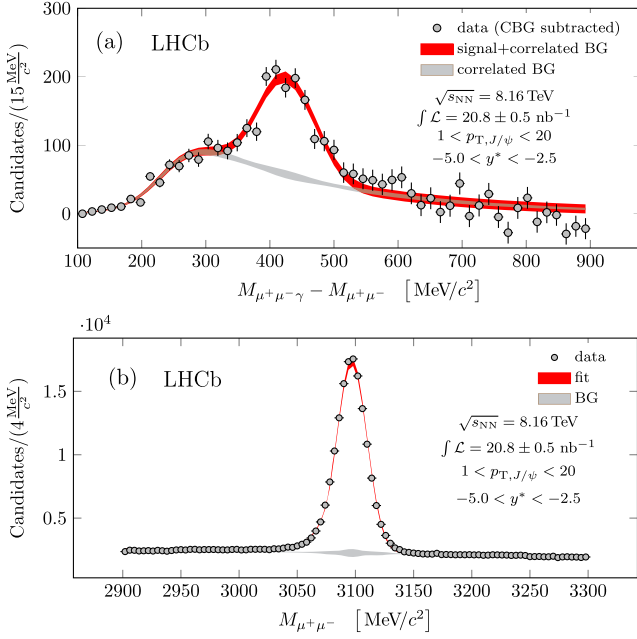


FIG. 1. (a) Difference in the invariant mass of the $\mu^+\mu^-\gamma$ and $\mu^+\mu^-$ combinations in the χ_c region. Here the fitted combinatorial background component has been subtracted from both the data points and the fitted curve. The gray band represents the correlated physics background component and the red band is the sum of the signal and correlated physics background components. The widths of the bands represent 68% C.L. (b) Invariant mass distribution of $\mu^+\mu^-$ pairs in the J/ψ mass region along with the fitted function.

fitting, minimizing the impact of the muon pair mass resolution. The shape of the combinatorial background distribution, $Y_{\text{CBG}}(\Delta M)$, is determined by mixing J/ψ decays and photons from different events. The two events must have similar track multiplicities and collision vertex positions. The overall combinatorial background yield N_{CBG} is determined by normalizing the CBG shape Y_{CBG} to have the same integral as the default sample in the mass region $700 < \Delta M < 900 \text{ MeV}/c^2$, where the signal and the correlated background are expected to be negligible. Figure 1(a) shows the ΔM distribution after the combinatorial background subtraction.

The correlated background is composed of radiative J/ψ decays ($J/\psi \rightarrow \mu^+\mu^-\gamma$) and partially reconstructed $\psi(2S) \rightarrow J/\psi\pi^0\pi^0 \rightarrow \mu^+\mu^-\gamma$ decays which are studied using simulated samples. The partially reconstructed $\psi(2S)$ contribution is 8 (30) times smaller than the J/ψ radiative decay at high (low) $p_{T,J/\psi}$ when considering its measured yield relative to J/ψ decays [12] and the branching ratio $\mathcal{B}[\psi(2S) \rightarrow J/\psi\pi^0\pi^0]$ [13]. The ΔM distribution accounting for the total correlated background is described by

$$Y_{\text{corr}}(\Delta M) = \frac{A_{\text{corr}} e^{B \cdot \Delta M}}{1 + e^{\frac{\Delta M - \Delta M_0}{\sigma_{\Delta M_b}}}}, \quad (2)$$

with $p_{T,\gamma}$ -dependent parameters B , ΔM_0 , and $\sigma_{\Delta M_b}$ initially determined from the simulation and A_{corr} is its normalization. The two χ_c states are described by the sum of two Gaussian functions, G , with a common resolution term as

$$Y_{\chi_c}(\Delta M) = f_{\chi_{c1}} G(\Delta M; \Delta M_{\chi_{c1}}, \sigma_{\Delta M}) + (1 - f_{\chi_{c1}}) \times G(\Delta M; \Delta M_{\chi_{c1}} + \Delta M_{1,2}, \sigma_{\Delta M}), \quad (3)$$

where $0.4 < f_{\chi_{c1}} < 0.6$ is the contribution of the χ_{c1} decay to the total χ_c yield as obtained in Ref. [16], $\Delta M_{\chi_{c1}} = M_{\chi_{c1}} - M_{J/\psi}$ is the free parameter accounting for the mass difference of the χ_{c1} state as measured by the detector, $\Delta M_{1,2} = 45.5 \text{ MeV}/c^2$ is the known mass difference between the χ_{c1} and χ_{c2} states [13]. The total shape of the ΔM distribution accounting for the χ_c signal and background is given by

$$Y_{\mu^+\mu^-\gamma}(\Delta M) = N_{\text{CBG}} Y_{\text{CBG}}(\Delta M) + N_{\text{corr}} Y_{\text{corr}}(\Delta M) + N_{\chi_c \rightarrow J/\psi\gamma} Y_{\chi_c}(\Delta M), \quad (4)$$

where N_{corr} is the yield of the correlated background. The signal yields are obtained with a maximum-likelihood fit to Eq. (4) to the ΔM distributions, including combinatorial background, with the initial parameters determined from simulation. The total χ_c yields, integrated over $p_{T,J/\psi}$, are $(11.8 \pm 0.6) \times 10^3$ and $(15.2 \pm 0.8) \times 10^3$ in the forward and backward rapidity samples, respectively. The χ_c yields are independently obtained in eight $p_{T,J/\psi}$ ranges and are stable with Gaussian variation of the initial parameters determined from simulation. Figure 1(a) shows the ΔM distribution, integrated over $p_{T,J/\psi}$, with the fit results overlaid. The fit for each $p_{T,J/\psi}$ range is shown in Ref. [26].

The J/ψ yield is determined in eight $p_{T,J/\psi}$ ranges using a maximum-likelihood fit to the $\mu\mu$ invariant mass distribution. The fitting function is defined by the sum of a Crystal Ball function, CB_{pdf} , [27] for signal and an exponential function for background

$$Y_{\mu^+\mu^-}(M) = A e^{bM} + N_{J/\psi} \text{CB}_{\text{pdf}}(M; M_{J/\psi}, \sigma_M, \alpha, n) \quad (5)$$

to the $\mu^+\mu^-$ invariant mass distribution using the log-likelihood method. The parameters A and b define the scale and slope of the exponential components. The parameters α and n are determined from a $p_{T,J/\psi}$ -integrated fit and fixed for the fits in different $p_{T,J/\psi}$ ranges. The parameter $M_{J/\psi}$ is fixed to the known value of the J/ψ mass [13]. The $p_{T,J/\psi}$ -integrated $\mu^+\mu^-$ distribution and the results of the fit are shown in Fig. 1(b). The distributions for each $p_{T,J/\psi}$ range is shown in Ref. [26].

Variation of the initial parameters when fitting the ΔM distribution and the fixed mass resolution parameter $\Delta\sigma_M$ cause the largest systematic uncertainties on the χ_c yields, mostly for the lowest $p_{T,J/\psi}$ interval. These variations

account for potential multiple local minima in the log-likelihood function used in the fits. Any deviation from the Gaussian shape assumption for the χ_c peaks is tested by comparing the yields obtained by fitting Eq. (4) and from the integral over $300 < \Delta M < 600$ MeV/ c^2 after subtracting the fitted background contributions $Y_{\text{CBG}} + Y_{\text{cont}}$. The difference between the yield obtained from the fit and the integral is assigned as a systematic uncertainty on the yield. The statistical uncertainties associated to the mixed J/ψ and γ event samples are negligible. However, variations on the mass range used to normalize the mixed event distribution Y_{CBG} contribute to the uncertainty in the χ_c yields. The only significant uncertainty in the J/ψ yield determination comes from the difference between the result obtained from the mass peak fitting and the integral over the J/ψ peak region after subtracting the background component.

The photon detection efficiency is the main contribution to the factor $\varepsilon_{\chi_c/J/\psi}$. A validation of the photon detection efficiency ε_γ is performed by studying partially reconstructed η decays in data and simulation. Clear peaks are observed in the $\pi^+\pi^-\gamma$ invariant mass distribution (well separated from the fully reconstructed $\eta \rightarrow \pi^+\pi^-\gamma$ peak) and the $\pi^+\pi^-$ mass distribution coming from $\eta \rightarrow \pi^+\pi^-(\pi^0 \rightarrow \gamma\gamma)$ and $\eta \rightarrow \pi^+\pi^-(\pi^0 \rightarrow \not{\gamma}\not{\gamma})$ decays, where $\not{\gamma}$ is a missing photon. The detection efficiency in η decays is measured in data and simulation by

$$\varepsilon_\gamma(p_{T,\gamma}) = \frac{N_{\eta \rightarrow \pi^+\pi^-(\pi^0 \rightarrow \gamma\gamma)}(p_{T,\gamma})}{\mathcal{M}_{\gamma(\pi\pi)} N_{\eta \rightarrow \pi^+\pi^-(\pi^0 \rightarrow \not{\gamma}\not{\gamma})}(p_{T,\pi^+\pi^-})}, \quad (6)$$

where $\mathcal{M}_{\gamma(\pi\pi)}$ is a matrix, obtained from simulation, that unfolds the $p_{T,\gamma}$ distribution from $\eta \rightarrow \pi^+\pi^-(\pi^0 \rightarrow \not{\gamma}\not{\gamma})$ decays as a function of $p_{T,\pi^+\pi^-}$. The efficiencies measured in data and simulation are consistent within 3% in the photon p_T range $400 < p_{T,\gamma} < 5000$ MeV/ c . Initial-state effects in the nucleus on the input kinematics are accounted for in simulation by weighting events according to the nuclear parton density function EPPS21 [28].

All the measurements assume χ_c production with zero polarization. The effects of a potential χ_c polarization on the detector efficiency are studied by weighting the simulated events according to different polarization scenarios as reported in Ref. [29]. The measured J/ψ polarization by LHCb [30] and the observation that either χ_{c1} or χ_{c2} states is strongly polarized by the CMS Collaboration [31] poses constraints to the scenarios adopted when weighting simulated events. The standard deviation of the $F_{\chi_c \rightarrow J/\psi}$ values after polarization weighting is taken as the systematic uncertainty.

Any potential B -meson decay contamination of the prompt J/ψ yield is checked by tightening the collision point and χ_c vertex association requirement, and the results are consistent with the default selection within the

TABLE I. Systematic uncertainty sources and maximum individual contributions.

Source	$1.5 < y^* < 4.0$	$-5.0 < y^* < -2.5$
Fit parameter initial values	<0.050	<0.058
Shape of χ_c	<0.056	<0.110
Shape of J/ψ	<0.002	<0.002
Mixed event normalization	<0.03	<0.010
Kinematic input in simulation	<0.012	<0.018
Photon efficiency	<0.030	<0.030
Polarization of χ_c	<0.031	<0.050

statistical uncertainties. Table I summarizes the maximum systematic uncertainty contributions. The largest uncertainties are found at the lowest $p_{T,J/\psi}$ range. The total systematic uncertainty corresponds to the standard deviation of the $F_{\chi_c \rightarrow J/\psi}$ results obtained from the different systematic uncertainty sources.

The $p_{T,J/\psi}$ -dependent values of $F_{\chi_c \rightarrow J/\psi}$ are shown in Fig. 2. The numerical results are shown in Ref. [26]. The points are located at the mean $p_{T,J/\psi}$ of each bin determined by a fit to the prompt J/ψ differential cross-section reported by the LHCb Collaboration in Ref. [32]. The new results are compared with those obtained in pp collisions at $\sqrt{s} = 7$ TeV [29]. The $F_{\chi_c \rightarrow J/\psi}$ results obtained in $p\text{Pb}$ and in pp collisions have an overall consistency. The fraction is slightly larger in the backward rapidity region for $p_{T,J/\psi} < 3$ GeV/ c . The result is also consistent with results obtained by the HERA-B experiment in $p\text{C}$ and $p\text{W}$ collisions at $\sqrt{s_{\text{NN}}} = 41.6$ GeV [14]. The HERA-B result covers a rapidity range $-5.2 < y^* < -2.2$ and $p_{T,J/\psi} < 2$ GeV/ c . A measurement of $F_{\chi_c \rightarrow J/\psi}$ was performed by the PHENIX Collaboration in $d\text{Au}$ collisions at $\sqrt{s_{\text{NN}}} = 200$ GeV [15], covering the midrapidity range (Center-of-mass and laboratory rapidities are the same in

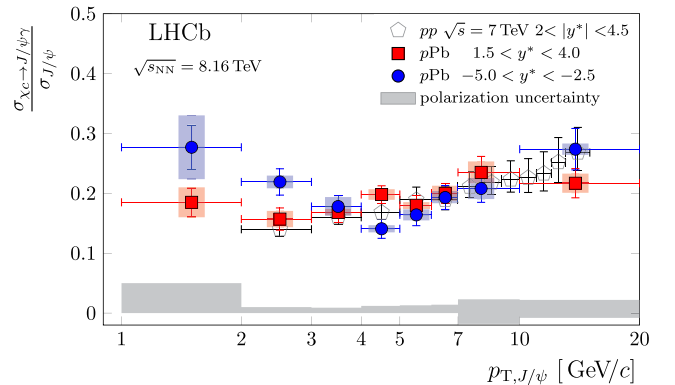


FIG. 2. Fraction of χ_c decays in the prompt J/ψ yield in $p\text{Pb}$ and pp collisions [29] as a function of $p_{T,J/\psi}$. The error bars show the statistical uncertainties. Boxes represent systematic uncertainties and the gray band represents the maximum uncertainties from χ_c and J/ψ polarization effects.

TABLE II. $F_{\chi_c \rightarrow J/\psi}$ results for wide $p_{T,J/\psi}$ bins. The two uncertainties are statistical and systematic, respectively.

$\{p_T/[GeV/c]\}$	$\{\langle p_T \rangle/[GeV/c]\}$	$1.5 < y^* < 4.0$	$-5.0 < y^* < -2.5$
1–3	1.9	$0.164 \pm 0.016 \pm 0.015$	$0.253 \pm 0.019 \pm 0.022$
2–20	3.9	$0.179 \pm 0.008 \pm 0.006$	$0.210 \pm 0.013 \pm 0.007$
3–20	5.0	$0.187 \pm 0.008 \pm 0.006$	$0.170 \pm 0.013 \pm 0.008$
1–20	3.2	$0.174 \pm 0.009 \pm 0.010$	$0.222 \pm 0.013 \pm 0.010$

TABLE III. Description of the double ratio measurements shown in Fig. 3.

Ratio	Reference	y^*	$\sqrt{s_{NN}}$	p_T
$[\psi(2S)/(J/\psi)]$	[12]	$[-5.0, -2.5]$	8.16 TeV	< 14 GeV/c
$[\chi_c/(J/\psi)]$	This Letter	$[-5.0, -2.5]$	8.16 TeV	$2 < p_{T,J/\psi} < 20$ GeV/c
$[(J/\psi)/D^0]$	[8]	$[-4.0, -2.5]$	5 TeV	< 10 GeV/c
$\{[\Upsilon(3S), \Upsilon(2S)]/\Upsilon(1S)\}$	[35]	$[-4.5, -2.5]$	8.16 TeV	< 25 GeV/c
$[\Upsilon(1S)/(B \rightarrow J/\psi)]$	[35]	$[-4.5, -2.5]$	8.16 TeV	< 25 GeV/c

the PHENIX measurement.) $|y^*| < 0.5$ and integrated over $p_{T,J/\psi}$, and is consistent with the $p_{T,J/\psi} < 2$ GeV/c result presented here, though the PHENIX measurement has large statistical uncertainties. The comparison with HERA-B and PHENIX is shown in Ref. [26].

The difference between the backward and forward rapidity results at low $p_{T,J/\psi}$ is further investigated by redoing the measurements using wide $p_{T,J/\psi}$ bins to reduce statistical and systematic uncertainties. Table II indicates that the fraction $F_{\chi_c \rightarrow J/\psi}$ at $p_{T,J/\psi} < 3$ GeV/c is 2.4σ larger at backward than at forward rapidity. This apparent increase can be attributed to the suppression of $\psi(2S)$ and other feed-down sources to the prompt J/ψ yield $\sigma_{J/\psi}$ in Eq. (1). The fraction of $\psi(2S)$ contribution to the prompt J/ψ yield is $(\sigma_{\psi(2S)}/\sigma_{J/\psi})\mathcal{B}(\psi(2S) \rightarrow J/\psi + X) = 0.080 \pm 0.011$ according to the cross section measured by the LHCb Collaboration in pp collisions at $\sqrt{s} = 7$ TeV [33,34] and the branching ratio from Ref. [13]. The $\sigma_{\psi(2S)}/\sigma_{J/\psi}$ ratio is reduced between pPb collisions at backward rapidity when compared to pp results [9–12], consistent with $F_{\chi_c \rightarrow J/\psi}$ being larger at backward rapidity.

The $F_{\chi_c \rightarrow J/\psi}$ result in pPb collisions suggests that neither J/ψ mesons, produced directly in the collisions, nor χ_c states are dissociated in the medium formed in pPb collisions, consistent with the similar nuclear modification factor measurement of J/ψ and D^0 yields in pPb collisions [8]. The nondissociation of the χ_c states leads to a constraint on the free energy (or temperature) of the system to be no larger than 180 MeV in pPb collisions, based on the smallest binding energy among the χ_c states. This maximum temperature is close to the estimated freeze-out temperature in pPb collisions, which ranges between 155–160 MeV [4–6]. The result presented here is integrated over collision centrality. Future studies selecting central events could be more sensitive to a short-lived hot medium in pPb collisions.

The most common method to quantify quarkonium dissociation in medium is the use of the quarkonium state yield ratios r relative to their corresponding ground state J/ψ for $c\bar{c}$ and $\Upsilon(1S)$ for $b\bar{b}$ or to an open heavy flavor meson (D^0 and B^+ for $c\bar{c}$ and $b\bar{b}$, respectively). The double ratio $\mathcal{R} = r_{pPb}/r_{pp}$ compares the r values between pp and pPb collisions. It is obtained for χ_c states from the $2 < p_{T,J/\psi} < 20$ GeV/c integrated result presented in Table II and a weighted average of the pp results presented in Ref. [29]. The double ratio $\mathcal{R}(\chi_c)$ is 1.10 ± 0.12 at forward rapidity and 1.29 ± 0.17 at backward rapidity. Figure 3 shows the binding-energy dependence of \mathcal{R} for all quarkonium states measured by the LHCb experiment in pPb collisions at backward rapidity, where pPb collisions achieve the highest particle multiplicities. The only dissociated ($\mathcal{R} < 1$) quarkonium state with binding energy above the freeze-out temperature is the $\Upsilon(3S)$. With a similar binding energy and size as the χ_c states, according to nonrelativistic potential theory [3], the $\Upsilon(3S)$ resonance

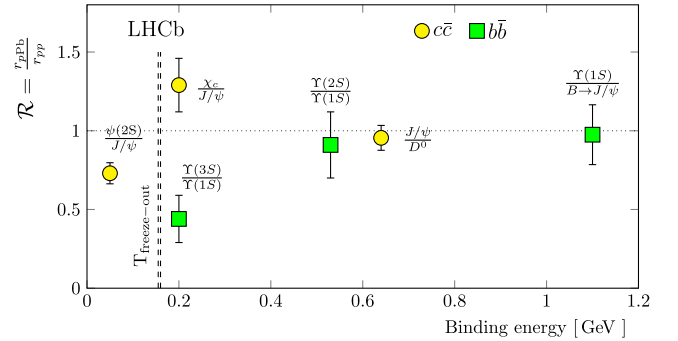


FIG. 3. Double ratio of the quarkonium state yield relative to its ground state or open heavy quark meson in pPb to pp collisions vs the binding energy of the given quarkonium state. The estimated freeze-out temperature in pPb collisions [4–6] is indicated. The details of the measurement for each data point in the figure are given in Table III.

is 2.9 times heavier and may travel the medium slower than the χ_c states favoring its dissociation by its interaction with comoving particles [7].

In summary, this Letter presents the first LHC measurement of the fraction of χ_c decays in the prompt J/ψ yield in heavy ion collisions. The ratio measured in p Pb collisions is consistent with no dissociation of χ_c states, indicating that the average free energy available in these collisions is not able to inhibit the formation of quarkonium states with binding energy equal or larger than 180 MeV. Such an energy is only 20–25 MeV larger than the expected freeze-out temperature estimated in these systems.

We express our gratitude to our colleagues in the CERN accelerator departments for the excellent performance of the LHC. We thank the technical and administrative staff at the LHCb institutes. We acknowledge support from CERN and from the national agencies: CAPES, CNPq, FAPERJ, and FINEP (Brazil); MOST and NSFC (China); CNRS/IN2P3 (France); BMBF, DFG, and MPG (Germany); INFN (Italy); NWO (Netherlands); MNiSW and NCN (Poland); MCID/IFA (Romania); MICINN (Spain); SNSF and SER (Switzerland); NASU (Ukraine); STFC (United Kingdom); DOE NP and NSF (USA). We acknowledge the computing resources that are provided by CERN, IN2P3 (France), KIT and DESY (Germany), INFN (Italy), SURF (Netherlands), PIC (Spain), GridPP (United Kingdom), CSCS (Switzerland), IFIN-HH (Romania), CBPF (Brazil), and Polish WLCG (Poland). We are indebted to the communities behind the multiple open-source software packages on which we depend. Individual groups or members have received support from ARC and ARDC (Australia); Key Research Program of Frontier Sciences of CAS, CAS PIFI, CAS CCEPP, Fundamental Research Funds for the Central Universities, and Sci. & Tech. Program of Guangzhou (China); Minciencias (Colombia); EPLANET, Marie Skłodowska-Curie Actions, ERC and NextGenerationEU (European Union); A*MIDEX, ANR, IPhU and Labex P2IO, and Région Auvergne-Rhône-Alpes (France); AvH Foundation (Germany); ICSC (Italy); GVA, XuntaGal, GENCAT, Inditex, InTalent, and Prog. Atracción Talento, CM (Spain); SRC (Sweden); the Leverhulme Trust, the Royal Society and UKRI (United Kingdom).

-
- [1] E. Annala, T. Gorda, A. Kurkela, J. Nättilä, and A. Vuorinen, Evidence for quark-matter cores in massive neutron stars, *Nat. Phys.* **16**, 907 (2020).
 [2] C. Aidala *et al.* (PHENIX Collaboration), Creation of quark–gluon plasma droplets with three distinct geometries, *Nat. Phys.* **15**, 214 (2019).
 [3] H. Satz, Colour deconfinement and quarkonium binding, *J. Phys. G* **32**, R25 (2006).

- [4] A. Bazavov *et al.* (HotQCD Collaboration), Chiral cross-over in QCD at zero and non-zero chemical potentials, *Phys. Lett. B* **795**, 15 (2019).
 [5] N. Sharma, J. Cleymans, B. Hippolyte, and M. Paradza, A comparison of p-p, p-Pb, Pb-Pb collisions in the thermal model: Multiplicity dependence of thermal parameters, *Phys. Rev. C* **99**, 044914 (2019).
 [6] F. A. Flor, G. Olinger, and R. Bellwied, System size and flavour dependence of chemical freeze-out temperatures in ALICE data from pp, pPb and PbPb collisions at LHC energies, *Phys. Lett. B* **834**, 137473 (2022).
 [7] E. G. Ferreira, Excited charmonium suppression in proton-nucleus collisions as a consequence of comovers, *Phys. Lett. B* **749**, 98 (2015).
 [8] R. Aaij *et al.* (LHCb Collaboration), Study of prompt D^0 meson production in p Pb collisions at $\sqrt{s_{NN}} = 5$ TeV, *J. High Energy Phys.* **10** (2017) 090.
 [9] U. A. Acharya *et al.* (PHENIX Collaboration), Measurement of $\psi(2S)$ nuclear modification at backward and forward rapidity in $p + p$, $p + \text{Al}$, and $p + \text{Au}$ collisions at $\sqrt{s_{NN}} = 200$ GeV, *Phys. Rev. C* **105**, 064912 (2022).
 [10] R. Aaij *et al.* (LHCb Collaboration), Study of $\psi(2S)$ production cross-sections and cold nuclear matter effects in p Pb collisions at $\sqrt{s_{NN}} = 5$ TeV, *J. High Energy Phys.* **03** (2016) 133.
 [11] B. B. Abelev *et al.* (ALICE Collaboration), Suppression of $\psi(2S)$ production in p-Pb collisions at $\sqrt{s_{NN}} = 5.02$ TeV, *J. High Energy Phys.* **12** (2014) 073.
 [12] R. Aaij *et al.* (LHCb Collaboration), Prompt and nonprompt $\psi(2S)$ production in p Pb collisions at $\sqrt{s_{NN}} = 8.16$ TeV, Report No. LHCb-PAPER-2023-024 [J. High Energy Phys. (to be published)].
 [13] R. L. Workman *et al.* (Particle Data Group), Review of particle physics, *Prog. Theor. Exp. Phys.* **2022**, 083C01 (2022).
 [14] I. Abt *et al.* (HERA-B Collaboration), Production of the charmonium states χ_{c1} and χ_{c2} in proton nucleus interactions at $\sqrt{s} = 41.6$ -GeV, *Phys. Rev. D* **79**, 012001 (2009).
 [15] A. Adare *et al.* (PHENIX Collaboration), Nuclear modification of ψ' , χ_c , and J/ψ production in d + Au collisions at $\sqrt{s_{NN}} = 200$ GeV, *Phys. Rev. Lett.* **111**, 202301 (2013).
 [16] R. Aaij *et al.* (LHCb Collaboration), Measurement of prompt-cross-section ratio $\sigma(\chi_{c2})/\sigma(\chi_{c1})$ in p Pb collisions at $\sqrt{s_{NN}} = 8.16$ TeV, *Phys. Rev. C* **103**, 064905 (2021).
 [17] A. A. Alves Jr. *et al.* (LHCb Collaboration), The LHCb detector at the LHC, *J. Instrum.* **3**, S08005 (2008).
 [18] R. Aaij *et al.* (LHCb Collaboration), LHCb detector performance, *Int. J. Mod. Phys. A* **30**, 1530022 (2015).
 [19] P. Perret, First Years of Running for the LHCb Calorimeter system, Report No. LHCb-PROC-2014-017, 2014.
 [20] R. Aaij *et al.*, Selection and processing of calibration samples to measure the particle identification performance of the LHCb experiment in Run 2, *Eur. Phys. J. Tech. Instrum.* **6**, 1 (2018).
 [21] T. Sjöstrand, S. Mrenna, and P. Skands, A brief introduction to PYTHIA8.1, *Comput. Phys. Commun.* **178**, 852 (2008).
 [22] T. Pierog, Iu. Karpenko, J. M. Katzy, E. Yatsenko, and K. Werner, EPOS LHC: Test of collective hadronization with

- data measured at the CERN Large Hadron Collider, *Phys. Rev. C* **92**, 034906 (2015).
- [23] D. J. Lange, The EvtGen particle decay simulation package, *Nucl. Instrum. Methods Phys. Res., Sect. A* **462**, 152 (2001).
- [24] P. Golonka and Z. Was, PHOTOS Monte Carlo: A precision tool for QED corrections in Z and W decays, *Eur. Phys. J. C* **45**, 97 (2006).
- [25] M. Clemencic, G. Corti, S. Easo, C. R. Jones, S. Miglioranza, M. Pappagallo, and P. Robbe, The LHCb simulation application, Gauss: Design, evolution and experience, *J. Phys. Conf. Ser.* **331**, 032023 (2011).
- [26] See Supplemental Material at <http://link.aps.org/supplemental/10.1103/PhysRevLett.132.102302> for detail.
- [27] T. Skwarnicki, A study of the radiative cascade transitions between the Upsilon-prime and Upsilon resonances, Ph.D. thesis, Institute of Nuclear Physics, Krakow, 1986, [Report No. DESY-F31-86-02].
- [28] K. J. Eskola, P. Paakkinen, H. Paukkunen, and C. A. Salgado, EPPS21: A global QCD analysis of nuclear PDFs, *Eur. Phys. J. C* **82**, 413 (2022).
- [29] R. Aaij *et al.* (LHCb Collaboration), Measurement of the ratio of prompt χ_c to J/ψ production in pp collisions at $\sqrt{s} = 7$ TeV, *Phys. Lett. B* **718**, 431 (2012).
- [30] R. Aaij *et al.* (LHCb Collaboration), Measurement of J/ψ polarization in pp collisions at $\sqrt{s} = 7$ TeV, *Eur. Phys. J. C* **73**, 2631 (2013).
- [31] A. M. Sirunyan *et al.* (CMS Collaboration), Constraints on the χ_{c1} versus χ_{c2} polarizations in proton-proton collisions at $\sqrt{s} = 8$ TeV, *Phys. Rev. Lett.* **124**, 162002 (2020).
- [32] R. Aaij *et al.* (LHCb Collaboration), Prompt and nonprompt J/ψ production and nuclear modification in pPb collisions at $\sqrt{s_{NN}} = 8.16$ TeV, *Phys. Lett. B* **774**, 159 (2017).
- [33] R. Aaij *et al.* (LHCb Collaboration), Measurement of J/ψ production in pp collisions at $\sqrt{s} = 7$ TeV, *Eur. Phys. J. C* **71**, 1645 (2011).
- [34] R. Aaij *et al.* (LHCb Collaboration), Measurement of $\psi(2S)$ meson production in pp collisions at $\sqrt{s} = 7$ TeV, *Eur. Phys. J. C* **72**, 2100 (2012); **80**, 49(E) (2020).
- [35] R. Aaij *et al.* (LHCb Collaboration), Study of Υ production in pPb collisions at $\sqrt{s_{NN}} = 8.16$ TeV, *J. High Energy Phys.* **11** (2018) 194.

R. Aaij³⁵, A. S. W. Abdelmotteleb⁵⁴, C. Abellan Beteta⁴⁸, F. Abudinén⁵⁴, T. Ackernley⁵⁸, B. Adeva⁴⁴, M. Adinolfi⁵², P. Adlarson⁷⁸, C. Agapopoulou⁴⁶, C. A. Aidala⁷⁹, Z. Ajaltouni¹¹, S. Akar⁶³, K. Akiba³⁵, P. Albicocco²⁵, J. Albrecht¹⁷, F. Alessio⁴⁶, M. Alexander⁵⁷, A. Alfonso Albero⁴³, Z. Aliouche⁶⁰, P. Alvarez Cartelle⁵³, R. Amalric¹⁵, S. Amato³, J. L. Amey⁵², Y. Amhis^{13,46}, L. An⁶, L. Anderlini²⁴, M. Andersson⁴⁸, A. Andreianov⁴¹, P. Andreola⁴⁸, M. Andreotti²³, D. Andreou⁶⁶, A. A. Anelli^{28,b}, D. Ao⁷, F. Archilli^{34,c}, M. Argenton²³, S. Argüedas Cuendis⁹, A. Artamonov⁴¹, M. Artuso⁶⁶, E. Aslanides¹², M. Atzeni⁶², B. Audurier¹⁴, D. Bacher⁶¹, I. Bachiller Perea¹⁰, S. Bachmann¹⁹, M. Bachmayer⁴⁷, J. J. Back⁵⁴, A. Bailly-reyre¹⁵, P. Baladron Rodriguez⁴⁴, V. Balagura¹⁴, W. Baldini²³, J. Baptista de Souza Leite², M. Barbetti^{24,d}, I. R. Barbosa⁶⁷, R. J. Barlow⁶⁰, S. Barsuk¹³, W. Barter⁵⁶, M. Bartolini⁵³, F. Baryshnikov⁴¹, J. M. Basels¹⁶, G. Bassi^{32,e}, B. Batsukh⁵, A. Battig¹⁷, A. Bay⁴⁷, A. Beck⁵⁴, M. Becker¹⁷, F. Bedeschi³², I. B. Bediaga², A. Beiter⁶⁶, S. Belin⁴⁴, V. Bellee⁴⁸, K. Belous⁴¹, I. Belov²⁶, I. Belyaev⁴¹, G. Benane¹², G. Bencivenni²⁵, E. Ben-Haim¹⁵, A. Berezhnoy⁴¹, R. Bernet⁴⁸, S. Bernet Andres⁴², H. C. Bernstein⁶⁶, C. Bertella⁶⁰, A. Bertolin³⁰, C. Betancourt⁴⁸, F. Betti⁵⁶, J. Bex⁵³, I. A. Bezshyiko⁴⁸, J. Bhom³⁸, M. S. Bieker¹⁷, N. V. Biesuz²³, P. Billoir¹⁵, A. Biolchini³⁵, M. Birch⁵⁹, F. C. R. Bishop¹⁰, A. Bitadze⁶⁰, A. Bizzeti³, M. P. Blago⁵³, T. Blake⁵⁴, F. Blanc⁴⁷, J. E. Blank¹⁷, S. Blusk⁶⁶, D. Bobulska⁵⁷, V. Bocharnikov⁴¹, J. A. Boelhave¹⁷, O. Boente Garcia¹⁴, T. Boettcher⁶³, A. Bohare⁵⁶, A. Boldyrev⁴¹, C. S. Bolognani⁷⁶, R. Bolzonella^{23,f}, N. Bondar⁴¹, F. Borgato^{30,46}, S. Borghi⁶⁰, M. Borsato^{28,b}, J. T. Borsuk³⁸, S. A. Bouchiba⁴⁷, T. J. V. Bowcock⁵⁸, A. Boyer⁴⁶, C. Bozzi²³, M. J. Bradley⁵⁹, S. Braun⁶⁴, A. Brea Rodriguez⁴⁴, N. Breer¹⁷, J. Brodzicka³⁸, A. Brossa Gonzalo⁴⁴, J. Brown⁵⁸, D. Brundu²⁹, A. Buonauro⁴⁸, L. Buonincontri³⁰, A. T. Burke⁶⁰, C. Burr⁴⁶, A. Bursche⁶⁹, A. Butkevich⁴¹, J. S. Butter⁵³, J. Buytaert⁴⁶, W. Byczynski⁴⁶, S. Cadeddu²⁹, H. Cai⁷¹, R. Calabrese^{23,f}, L. Calefice¹⁷, S. Cali²⁵, M. Calvi^{28,b}, M. Calvo Gomez⁴², J. Cambon Bouzas⁴⁴, P. Campana²⁵, D. H. Campora Perez⁷⁶, A. F. Campoverde Quezada⁷, S. Capelli^{28,b}, L. Capriotti²³, R. Caravaca-Mora⁹, A. Carbone^{22,g}, L. Carcedo Salgado⁴⁴, R. Cardinale^{26,h}, A. Cardini²⁹, P. Carniti^{28,b}, L. Carus¹⁹, A. Casais Vidal⁶², R. Caspary¹⁹, G. Casse⁵⁸, J. Castro Godinez⁹, M. Cattaneo⁴⁶, G. Cavallero²³, V. Cavallini^{23,f}, S. Celani⁴⁷, J. Cerasoli¹², D. Cervenkov⁶¹, S. Cesare^{27,i}, A. J. Chadwick⁵⁸, I. Chahrouh⁷⁹, M. Charles¹⁵, Ph. Charpentier⁴⁶, C. A. Chavez Barajas⁵⁸, M. Chefdeville¹⁰, C. Chen¹², S. Chen⁵, A. Chernov³⁸, S. Chernyshenko⁵⁰, V. Chobanova^{44,j}, S. Cholak⁴⁷, M. Chruszcz³⁸, A. Chubykin⁴¹, V. Chulikov⁴¹, P. Ciambone²⁵, M. F. Cicala⁵⁴, X. Cid Vidal⁴⁴, G. Ciezarek⁴⁶, P. Cifra⁴⁶, P. E. L. Clarke⁵⁶

M. Clemencic⁴⁶ H. V. Cliff⁵³ J. Closier⁴⁶ J. L. Cobbedick⁶⁰ C. Cocha Toapaxi¹⁹ V. Cocco⁴⁶ J. Cogan¹²
 E. Cogneras¹¹ L. Cojocariu⁴⁰ P. Collins⁴⁶ T. Colombo⁴⁶ A. Comerma-Montells⁴³ L. Congedo²¹ A. Contu²⁹
 N. Cooke⁵⁷ I. Corredoira⁴⁴ A. Correia¹⁵ G. Corti⁴⁶ J. J. Cottee Meldrum⁵² B. Couturier⁴⁶ D. C. Craik⁴⁸
 M. Cruz Torres^{2,k} R. Currie⁵⁶ C. L. Da Silva⁶⁵ S. Dadabaev⁴¹ L. Dai⁶⁸ X. Dai⁶ E. Dall’Occo¹⁷
 J. Dalseno⁴⁴ C. D’Ambrosio⁴⁶ J. Daniel¹¹ A. Danilina⁴¹ P. d’Argent²¹ A. Davidson⁵⁴ J. E. Davies⁶⁰
 A. Davis⁶⁰ O. De Aguiar Francisco⁶⁰ C. De Angelis^{29,1} J. de Boer³⁵ K. De Bruyn⁷⁵ S. De Capua⁶⁰
 M. De Cian^{19,46} U. De Freitas Carneiro Da Graca^{2,m} E. De Lucia²⁵ J. M. De Miranda² L. De Paula³
 M. De Serio^{21,n} D. De Simone⁴⁸ P. De Simone²⁵ F. De Vellis¹⁷ J. A. de Vries⁷⁶ F. Debernardis^{21,n}
 D. Decamp¹⁰ V. Dedu¹² L. Del Buono¹⁵ B. Delaney⁶² H.-P. Dembinski¹⁷ J. Deng⁸ V. Denysenko⁴⁸
 O. Deschamps¹¹ F. Dettori^{29,1} B. Dey⁷⁴ P. Di Nezza²⁵ I. Diachkov⁴¹ S. Didenko⁴¹ S. Ding⁶⁶
 V. Dobishuk⁵⁰ A. D. Docheva⁵⁷ A. Dolmatov⁴¹ C. Dong⁴ A. M. Donohoe²⁰ F. Dordei²⁹ A. C. dos Reis²
 L. Douglas⁵⁷ A. G. Downes¹⁰ W. Duan⁶⁹ P. Duda⁷⁷ M. W. Dudek³⁸ L. Dufour⁴⁶ V. Duk³¹ P. Durante⁴⁶
 M. M. Duras⁷⁷ J. M. Durham⁶⁵ A. Dziurda³⁸ A. Dzyuba⁴¹ S. Easo^{55,46} E. Eckstein⁷³ U. Egede¹
 A. Egorychev⁴¹ V. Egorychev⁴¹ C. Eirea Orro⁴⁴ S. Eisenhardt⁵⁶ E. Ejopu⁶⁰ S. Ek-In⁴⁷ L. Eklund⁷⁸
 M. Elashri⁶³ J. Ellbracht¹⁷ S. Ely⁵⁹ A. Ene⁴⁰ E. Epple⁶³ S. Escher¹⁶ J. Eschle⁴⁸ S. Esen⁴⁸ T. Evans⁶⁰
 F. Fabiano^{29,46,1} L. N. Falcao² Y. Fan⁷ B. Fang^{71,13} L. Fantini^{31,o} M. Faria⁴⁷ K. Farmer⁵⁶ D. Fazzini^{28,b}
 L. Felkowski⁷⁷ M. Feng^{5,7} M. Feo⁴⁶ M. Fernandez Gomez⁴⁴ A. D. Fernez⁶⁴ F. Ferrari²²
 F. Ferreira Rodrigues³ S. Ferreres Sole³⁵ M. Ferrillo⁴⁸ M. Ferro-Luzzi⁴⁶ S. Filippov⁴¹ R. A. Fini²¹
 M. Fiorini^{23,f} M. Firlej³⁷ K. M. Fischer⁶¹ D. S. Fitzgerald⁷⁹ C. Fitzpatrick⁶⁰ T. Fiutowski³⁷ F. Fleuret¹⁴
 M. Fontana²² F. Fontanelli^{26,h} L. F. Foreman⁶⁰ R. Forty⁴⁶ D. Foulds-Holt⁵³ M. Franco Sevilla⁶⁴ M. Frank⁴⁶
 E. Franzoso^{23,f} G. Frau¹⁹ C. Frei⁴⁶ D. A. Friday⁶⁰ L. Frontini^{27,i} J. Fu⁷ Q. Fuehring¹⁷ Y. Fujii¹
 T. Fulghesu¹⁵ E. Gabriel³⁵ G. Galati^{21,n} M. D. Galati³⁵ A. Gallas Torreira⁴⁴ D. Galli^{22,g} S. Gambetta^{56,46}
 M. Gandelman³ P. Gandini²⁷ H. Gao⁷ R. Gao⁶¹ Y. Gao⁸ Y. Gao⁶ Y. Gao⁸ M. Garau^{29,1}
 L. M. Garcia Martin⁴⁷ P. Garcia Moreno⁴³ J. García Pardiñas⁴⁶ B. Garcia Plana⁴⁴ K. G. Garg⁸ L. Garrido⁴³
 C. Gaspar⁴⁶ R. E. Geertsema³⁵ L. L. Gerken¹⁷ E. Gersabeck⁶⁰ M. Gersabeck⁶⁰ T. Gershon⁵⁴
 Z. Ghorbanimoghaddam⁵² L. Giambastiani³⁰ F. I. Giasemis^{15,p} V. Gibson⁵³ H. K. Gienza³⁹ A. L. Gilman⁶¹
 M. Giovannetti²⁵ A. Gioventù⁴³ P. Gironella Gironell⁴³ C. Giugliano^{23,f} M. A. Giza³⁸ E. L. Gkougkousis⁵⁹
 F. C. Glaser^{13,19} V. V. Gligorov¹⁵ C. Göbel⁶⁷ E. Golobardes⁴² D. Golubkov⁴¹ A. Golutvin^{59,41,46}
 A. Gomes^{2,a,q} S. Gomez Fernandez⁴³ F. Goncalves Abrantes⁶¹ M. Goncerz³⁸ G. Gong⁴ J. A. Gooding¹⁷
 I. V. Gorelov⁴¹ C. Gotti²⁸ J. P. Grabowski⁷³ L. A. Granado Cardoso⁴⁶ E. Graugés⁴³ E. Graverini⁴⁷
 L. Grazette⁵⁴ G. Graziani⁴⁰ A. T. Grecu⁴⁰ L. M. Greeven³⁵ N. A. Grieser⁶³ L. Grillo⁵⁷ S. Gromov⁴¹ C. Gu¹⁴
 M. Guarise²³ M. Guittiere¹³ V. Guliaeva⁴¹ P. A. Günther¹⁹ A.-K. Guseinov⁴¹ E. Gushchin⁴¹ Y. Guz^{6,41,46}
 T. Gys⁴⁶ T. Hadavizadeh¹ C. Hadjivasiliou⁶⁴ G. Haefeli⁴⁷ C. Haen⁴⁶ J. Haimberger⁴⁶ M. Hajheidari⁴⁶
 T. Halewood-leagas⁵⁸ M. M. Halvorsen⁴⁶ P. M. Hamilton⁶⁴ J. Hammerich⁵⁸ Q. Han⁸ X. Han¹⁹
 S. Hansmann-Menzemer¹⁹ L. Hao⁷ N. Harnew⁶¹ T. Harrison⁵⁸ M. Hartmann¹³ C. Hasse⁴⁶ J. He^{7,r}
 K. Heijhoff³⁵ F. Hemmer⁴⁶ C. Henderson⁶³ R. D. L. Henderson^{1,54} A. M. Hennequin⁴⁶ K. Hennessy⁵⁸
 L. Henry⁴⁷ J. Herd⁵⁹ J. Heuel¹⁶ A. Hicheur³ D. Hill⁴⁷ S. E. Hollitt¹⁷ J. Horswill⁶⁰ R. Hou⁸ Y. Hou¹⁰
 N. Howarth⁵⁸ J. Hu¹⁹ J. Hu⁶⁹ W. Hu⁶ X. Hu⁴ W. Huang⁷ W. Hulsbergen³⁵ R. J. Hunter⁵⁴ M. Hushchyn⁴¹
 D. Hutchcroft⁵⁸ M. Idzik³⁷ D. Ilin⁴¹ P. Ilten⁶³ A. Inglessi⁴¹ A. Iniukhin⁴¹ A. Ishteev⁴¹ K. Ivshin⁴¹
 R. Jacobsson⁴⁶ H. Jage¹⁶ S. J. Jaimes Elles^{45,72} S. Jakobsen⁴⁶ E. Jans³⁵ B. K. Jashal⁴⁵ A. Jawahery⁶⁴
 V. Jevtic¹⁷ E. Jiang⁶⁴ X. Jiang^{5,7} Y. Jiang⁷ Y. J. Jiang⁶ M. John⁶¹ D. Johnson⁵¹ C. R. Jones⁵³
 T. P. Jones⁵⁴ S. Joshi³⁹ B. Jost⁴⁶ N. Jurik⁴⁶ I. Juszczak³⁸ D. Kaminaris⁴⁷ S. Kandybei⁴⁹ Y. Kang⁴
 M. Karacson⁴⁶ D. Karpenkov⁴¹ M. Karpov⁴¹ A. M. Kauniskangas⁴⁷ J. W. Kautz⁶³ F. Keizer⁴⁶
 D. M. Keller⁶⁶ M. Kenzie⁵³ T. Ketel³⁵ B. Khanji⁶⁶ A. Kharisova⁴¹ S. Kholodenko³² G. Khreich¹³
 T. Kirn¹⁶ V. S. Kirsebom⁴⁷ O. Kitouni⁶² S. Klaver³⁶ N. Kleijne^{32,e} K. Klimaszewski³⁹ M. R. Kmiec³⁹
 S. Koliiev⁵⁰ L. Kolk¹⁷ A. Konoplyannikov⁴¹ P. Kopciwicz^{37,46} P. Koppenburg³⁵ M. Korolev⁴¹ I. Kostiuk³⁵
 O. Kot⁵⁰ S. Kotriakhova⁴¹ A. Kozachuk⁴¹ P. Kravchenko⁴¹ L. Kravchuk⁴¹ M. Kreps⁵⁴ S. Kretzschmar¹⁶
 P. Krokovny⁴¹ W. Krupa⁶⁶ W. Krzemien³⁹ J. Kubat¹⁹ S. Kubis⁷⁷ W. Kucewicz³⁸ M. Kucharczyk³⁸
 V. Kudryavtsev⁴¹ E. Kulikova⁴¹ A. Kupsc⁷⁸ B. K. Kutsenko¹² D. Lacarrere⁴⁶ A. Lai²⁹ A. Lampis²⁹

D. Lancierini⁴⁸ C. Landesa Gomez⁴⁴ J. J. Lane¹ R. Lane⁵² C. Langenbruch¹⁹ J. Langer¹⁷ O. Lantwin⁴¹
T. Latham⁵⁴ F. Lazzari^{32,s} C. Lazzeroni⁵¹ R. Le Gac¹² S. H. Lee⁷⁹ R. Lefèvre¹¹ A. Leflat⁴¹ S. Legotin⁴¹
M. Lehuraux⁵⁴ O. Leroy¹² T. Lesiak³⁸ B. Leverington¹⁹ A. Li⁴ H. Li⁶⁹ K. Li⁸ L. Li⁶⁰ P. Li⁴⁶
P.-R. Li⁷⁰ S. Li⁸ T. Li⁵ T. Li⁶⁹ Y. Li⁸ Y. Li⁵ Z. Li⁶⁶ Z. Lian⁴ X. Liang⁶⁶ C. Lin⁷ T. Lin⁵⁵
R. Lindner⁴⁶ V. Lisovskyi⁴⁷ R. Litvinov^{29,i} G. Liu⁶⁹ H. Liu⁷ K. Liu⁷⁰ Q. Liu⁷ S. Liu^{5,7} Y. Liu⁵⁶
Y. Liu⁷⁰ Y. L. Liu⁵⁹ A. Lobo Salvia⁴³ A. Loi²⁹ J. Lomba Castro⁴⁴ T. Long⁵³ J. H. Lopes³
A. Lopez Huertas⁴³ S. López Soliño⁴⁴ G. H. Lovell⁵³ C. Lucarelli^{24,d} D. Lucchesi^{30,t} S. Luchuk⁴¹
M. Lucio Martinez⁷⁶ V. Lukashenko^{35,50} Y. Luo⁴ A. Lupato³⁰ E. Luppi^{23,f} K. Lynch²⁰ X.-R. Lyu⁷
G. M. Ma⁴ R. Ma⁷ S. Maccolini¹⁷ F. Machefert¹³ F. Maciuc⁴⁰ I. Mackay⁶¹ L. R. Madhan Mohan⁵³
M. M. Madurai⁵¹ A. Maevskiy⁴¹ D. Magdalinski³⁵ D. Maisuzenko⁴¹ M. W. Majewski³⁷ J. J. Malczewski³⁸
S. Malde⁶¹ B. Malecki^{38,46} L. Malentacca⁴⁶ A. Malinin⁴¹ T. Maltsev⁴¹ G. Manca^{29,1} G. Mancinelli¹²
C. Mancuso^{27,13,i} R. Manera Escalero⁴³ D. Manuzzi²² D. Marangotto^{27,i} J. F. Marchand¹⁰ R. Marchevski⁴⁷
U. Marconi²² S. Mariani⁴⁶ C. Marin Benito^{43,46} J. Marks¹⁹ A. M. Marshall⁵² P. J. Marshall⁵⁸ G. Martelli^{31,o}
G. Martellotti³³ L. Martinazzoli⁴⁶ M. Martinelli^{28,b} D. Martinez Santos⁴⁴ F. Martinez Vidal⁴⁵ A. Massafferri²
M. Materok¹⁶ R. Matev⁴⁶ A. Mathad⁴⁸ V. Matiunin⁴¹ C. Matteuzzi⁶⁶ K. R. Mattioli¹⁴ A. Mauri⁵⁹
E. Maurice¹⁴ J. Mauricio⁴³ P. Mayencourt⁴⁷ M. Mazurek⁴⁶ M. McCann⁵⁹ L. Mcconnell²⁰ T. H. McGrath⁶⁰
N. T. McHugh⁵⁷ A. McNab⁶⁰ R. McNulty²⁰ B. Meadows⁶³ G. Meier¹⁷ D. Melnychuk³⁹ M. Merk^{35,76}
A. Merli^{27,i} L. Meyer Garcia³ D. Miao^{5,7} H. Miao⁷ M. Mikhasenko^{73,u} D. A. Milanes⁷² A. Minotti^{28,b}
E. Minucci⁶⁶ T. Miralles¹¹ S. E. Mitchell⁵⁶ B. Mitreska¹⁷ D. S. Mitzel¹⁷ A. Modak⁵⁵ A. Mödden¹⁷
R. A. Mohammed⁶¹ R. D. Moise¹⁶ S. Mokhnenko⁴¹ T. Mombächer⁴⁶ M. Monk^{54,1} I. A. Monroy⁷²
S. Monteil¹¹ A. Morcillo Gomez⁴⁴ G. Morello²⁵ M. J. Morello^{32,e} M. P. Morgenthaler¹⁹ J. Moron³⁷
A. B. Morris⁴⁶ A. G. Morris¹² R. Mountain⁶⁶ H. Mu⁴ Z. M. Mu⁶ E. Muhammad⁵⁴ F. Muheim⁵⁶
M. Mulder⁷⁵ K. Müller⁴⁸ F. Muñoz-Rojas⁹ R. Murta⁵⁹ P. Naik⁵⁸ T. Nakada⁴⁷ R. Nandakumar⁵⁵
T. Nanut⁴⁶ I. Nasteva³ M. Needham⁵⁶ N. Neri^{27,i} S. Neubert⁷³ N. Neufeld⁴⁶ P. Neustroev⁴¹ R. Newcombe⁵⁹
J. Nicolini^{17,13} D. Nicotra⁷⁶ E. M. Niel⁴⁷ N. Nikitin⁴¹ P. Nogga⁷³ N. S. Nolte⁶² C. Normand^{10,29,1}
J. Novoa Fernandez⁴⁴ G. Nowak⁶³ C. Nunez⁷⁹ H. N. Nur⁵⁷ A. Oblakowska-Mucha³⁷ V. Obraztsov⁴¹
T. Oeser¹⁶ S. Okamura^{23,46,f} R. Oldeman^{29,1} F. Oliva⁵⁶ M. Olocco¹⁷ C. J. G. Onderwater⁷⁶ R. H. O'Neil⁵⁶
J. M. Otorola Goicochea³ T. Ovsianikova⁴¹ P. Owen⁴⁸ A. Oyanguren⁴⁵ O. Ozcelik⁵⁶ K. O. Padeken⁷³
B. Pagare⁵⁴ P. R. Pais¹⁹ T. Pajero⁶¹ A. Palano²¹ M. Palutan²⁵ G. Panshin⁴¹ L. Paolucci⁵⁴ A. Papanestis⁵⁵
M. Pappagallo^{21,n} L. L. Pappalardo^{23,f} C. Pappenheimer⁶³ C. Parkes⁶⁰ B. Passalacqua^{23,f} G. Passaleva²⁴
D. Passaro^{32,e} A. Pastore²¹ M. Patel⁵⁹ J. Patoc⁶¹ C. Patrignani^{22,g} C. J. Pawley⁷⁶ A. Pellegrino³⁵
M. Pepe Altarelli²⁵ S. Perazzini²² D. Pereima⁴¹ A. Pereiro Castro⁴⁴ P. Perret¹¹ A. Perro⁴⁶ K. Petridis⁵²
A. Petrolini^{26,h} S. Petrucci⁵⁶ H. Pham⁶⁶ L. Pica^{32,e} M. Piccini³¹ B. Pietrzyk¹⁰ G. Pietrzyk¹³ D. Pinci³³
F. Pisani⁴⁶ M. Pizzichemi^{28,b} V. Placinta⁴⁰ M. Plo Casaus⁴⁴ F. Polci^{15,46} M. Poli Lener²⁵ A. Poluektov¹²
N. Polukhina⁴¹ I. Polyakov⁴⁶ E. Polycarpo³ S. Ponce⁴⁶ D. Popov⁷ S. Poslavskii⁴¹ K. Prasanth³⁸
C. Prouve⁴⁴ V. Pugatch⁵⁰ V. Puill¹³ G. Punzi^{32,s} H. R. Qi⁴ W. Qian⁷ N. Qin⁴ S. Qu⁴ R. Quagliani⁴⁷
R. I. Rabadan Trejo⁵⁴ B. Rachwal³⁷ J. H. Rademacker⁵² M. Rama³² M. Ramírez García⁷⁹ M. Ramos Pernas⁵⁴
M. S. Rangel³ F. Ratnikov⁴¹ G. Raven³⁶ M. Rebollo De Miguel⁴⁵ F. Redi⁴⁶ J. Reich⁵² F. Reiss⁶⁰ Z. Ren⁷
P. K. Resmi⁶¹ R. Ribatti^{32,e} G. R. Ricart^{14,80} D. Riccardi^{32,e} S. Ricciardi⁵⁵ K. Richardson⁶²
M. Richardson-Slipper⁵⁶ K. Rinnert⁵⁸ P. Robbe¹³ G. Robertson⁵⁷ E. Rodrigues^{58,46} E. Rodriguez Fernandez⁴⁴
J. A. Rodriguez Lopez⁷² E. Rodriguez Rodriguez⁴⁴ A. Rogovskiy⁵⁵ D. L. Rolf⁴⁶ A. Rollings⁶¹ P. Roloff⁴⁶
V. Romanovskiy⁴¹ M. Romero Lamas⁴⁴ A. Romero Vidal⁴⁴ G. Romolini²³ F. Ronchetti⁴⁷ M. Rotondo²⁵
S. R. Roy¹⁹ M. S. Rudolph⁶⁶ T. Ruf⁴⁶ M. Ruiz Diaz¹⁹ R. A. Ruiz Fernandez⁴⁴ J. Ruiz Vidal^{78,v}
A. Ryzhikov⁴¹ J. Ryzka³⁷ J. J. Saborido Silva⁴⁴ R. Sadek¹⁴ N. Sagidova⁴¹ N. Sahoo⁵¹ B. Saitta^{29,1}
M. Salomoni^{28,b} C. Sanchez Gras³⁵ I. Sanderswood⁴⁵ R. Santacesaria³³ C. Santamarina Rios⁴⁴
M. Santimaria²⁵ L. Santoro² E. Santovetti³⁴ A. Saputi^{23,46} D. Saranin⁴¹ G. Sarpis⁵⁶ M. Sarpis⁷³ A. Sarti³³
C. Satriano^{33,w} A. Satta³⁴ M. Saur⁶ D. Savrina⁴¹ H. Sazak¹¹ L. G. Scantlebury Smead⁶¹ A. Scarabotto¹⁵
S. Schael¹⁶ S. Scherl⁵⁸ A. M. Schertz⁷⁴ M. Schiller⁵⁷ H. Schindler⁴⁶ M. Schmelling¹⁸ B. Schmidt⁴⁶
S. Schmitt¹⁶ H. Schmitz⁷³ O. Schneider⁴⁷ A. Schopper⁴⁶ N. Schulte¹⁷ S. Schulte⁴⁷ M. H. Schune¹³

R. Schwemmer⁴⁶, G. Schwering¹⁶, B. Sciascia²⁵, A. Sciuccati⁴⁶, S. Sellam⁴⁴, A. Semennikov⁴¹,
M. Senghi Soares³⁶, A. Sergi^{26,h}, N. Serra^{48,46}, L. Sestini³⁰, A. Seuthe¹⁷, Y. Shang⁶, D. M. Shangase⁷⁹,
M. Shapkin⁴¹, I. Shchemerov⁴¹, L. Shchutskaya⁴⁷, T. Shears⁵⁸, L. Shekhtman⁴¹, Z. Shen⁶, S. Sheng^{5,7},
V. Shevchenko⁴¹, B. Shi⁷, E. B. Shields^{28,b}, Y. Shimizu¹³, E. Shmanin⁴¹, R. Shorkin⁴¹, J. D. Shupperd⁶⁶,
R. Silva Coutinho⁶⁶, G. Simi³⁰, S. Simone^{21,n}, N. Skidmore⁶⁰, R. Skuza¹⁹, T. Skwarnicki⁶⁶, M. W. Slater⁵¹,
J. C. Smallwood⁶¹, E. Smith⁶², K. Smith⁶⁵, M. Smith⁵⁹, A. Snoch³⁵, L. Soares Lavra⁵⁶, M. D. Sokoloff⁶³,
F. J. P. Soler⁵⁷, A. Solomin^{41,52}, A. Solovov⁴¹, I. Solovyev⁴¹, R. Song¹, Y. Song⁴⁷, Y. Song⁴, Y. S. Song⁶,
F. L. Souza De Almeida⁶⁶, B. Souza De Paula³, E. Spadaro Norella^{27,i}, E. Spedicato²², J. G. Speer¹⁷,
E. Spiridenkov⁴¹, P. Spradlin⁵⁷, V. Sriskaran⁴⁶, F. Stagni⁴⁶, M. Stahl⁴⁶, S. Stahl⁴⁶, S. Stanislaus⁶¹, E. N. Stein⁴⁶,
O. Steinkamp⁴⁸, O. Stenyakin⁴¹, H. Stevens¹⁷, D. Strelakina⁴¹, Y. Su⁷, F. Suljik⁶¹, J. Sun²⁹, L. Sun⁷¹, Y. Sun⁶⁴,
P. N. Swallow⁵¹, K. Swientek³⁷, F. Swystun⁵⁴, A. Szabelski³⁹, T. Szumlak³⁷, M. Szymanski⁴⁶, Y. Tan⁴,
S. Taneja⁶⁰, M. D. Tat⁶¹, A. Terentev⁴⁸, F. Terzuoli^{32,x}, F. Teubert⁴⁶, E. Thomas⁴⁶, D. J. D. Thompson⁵¹,
H. Tilquin⁵⁹, V. Tisserand¹¹, S. T'Jampens¹⁰, M. Tobin⁵, L. Tomassetti^{23,f}, G. Tonani^{27,i}, X. Tong⁶,
D. Torres Machado², L. Toscano¹⁷, D. Y. Tou⁴, C. Trippel⁴², G. Tuci¹⁹, N. Tuning³⁵, L. H. Uecker¹⁹,
A. Ukleja³⁷, D. J. Unverzagt¹⁹, E. Ursov⁴¹, A. Usachov³⁶, A. Ustyuzhanin⁴¹, U. Uwer¹⁹, V. Vagnoni²²,
A. Valassi⁴⁶, G. Valenti²², N. Valls Canudas⁴², H. Van Hecke⁶⁵, E. van Herwijnen⁵⁹, C. B. Van Hulse^{44,y},
R. Van Laak⁴⁷, M. van Veghel³⁵, R. Vazquez Gomez⁴³, P. Vazquez Regueiro⁴⁴, C. Vázquez Sierra⁴⁴, S. Vecchi²³,
J. J. Velthuis⁵², M. Veltri^{24,z}, A. Venkateswaran⁴⁷, M. Vesterinen⁵⁴, D. Vieira⁶³, M. Vieites Diaz⁴⁶,
X. Vilasis-Cardona⁴², E. Vilella Figueras⁵⁸, A. Villa²², P. Vincent¹⁵, F. C. Volle¹³, D. vom Bruch¹², V. Vorobyev⁴¹,
N. Voropaev⁴¹, K. Vos⁷⁶, G. Vouters¹⁰, C. Vrahas⁵⁶, J. Walsh³², E. J. Walton¹, G. Wan⁶, C. Wang¹⁹, G. Wang⁸,
J. Wang⁶, J. Wang⁵, J. Wang⁴, J. Wang⁷¹, M. Wang²⁷, N. W. Wang⁷, R. Wang⁵², X. Wang⁶⁹, X. W. Wang⁵⁹,
Y. Wang⁸, Z. Wang¹³, Z. Wang⁴, Z. Wang⁷, J. A. Ward^{54,1}, N. K. Watson⁵¹, D. Websdale⁵⁹, Y. Wei⁶,
B. D. C. Westhenry⁵², D. J. White⁶⁰, M. Whitehead⁵⁷, A. R. Wiederhold⁵⁴, D. Wiedner¹⁷, G. Wilkinson⁶¹,
M. K. Wilkinson⁶³, M. Williams⁶², M. R. J. Williams⁵⁶, R. Williams⁵³, F. F. Wilson⁵⁵, W. Wislicki³⁹,
M. Witek³⁸, L. Witola¹⁹, C. P. Wong⁶⁵, G. Wormser¹³, S. A. Wotton⁵³, H. Wu⁶⁶, J. Wu⁸, Y. Wu⁶, K. Wyllie⁴⁶,
S. Xian⁶⁹, Z. Xiang⁵, Y. Xie⁸, A. Xu³², J. Xu⁷, L. Xu⁴, L. Xu⁴, M. Xu⁵⁴, Z. Xu¹¹, Z. Xu⁷, Z. Xu⁵,
D. Yang⁴, S. Yang⁷, X. Yang⁶, Y. Yang^{26,h}, Z. Yang⁶, Z. Yang⁶⁴, V. Yeroshenko¹³, H. Yeung⁶⁰, H. Yin⁸,
C. Y. Yu⁶, J. Yu⁶, X. Yuan⁵, E. Zaffaroni⁴⁷, M. Zavertyaev¹⁸, M. Zdybal³⁸, M. Zeng⁴, C. Zhang⁶,
D. Zhang⁸, J. Zhang⁷, L. Zhang⁴, S. Zhang⁶⁸, S. Zhang⁶, Y. Zhang⁶, Y. Zhang⁶¹, Y. Z. Zhang⁴, Y. Zhao¹⁹,
A. Zharkova⁴¹, A. Zhelezov¹⁹, X. Z. Zheng⁴, Y. Zheng⁷, T. Zhou⁶, X. Zhou⁸, Y. Zhou⁷, V. Zhovkovska⁵⁴,
L. Z. Zhu⁷, X. Zhu⁴, X. Zhu⁸, Z. Zhu⁷, V. Zhukov^{16,41}, J. Zhuo⁴⁵, Q. Zou^{5,7}, D. Zuliani³⁰ and G. Zunica⁶⁰

(LHCb Collaboration)

¹School of Physics and Astronomy, Monash University, Melbourne, Australia

²Centro Brasileiro de Pesquisas Físicas (CBPF), Rio de Janeiro, Brazil

³Universidade Federal do Rio de Janeiro (UFRJ), Rio de Janeiro, Brazil

⁴Center for High Energy Physics, Tsinghua University, Beijing, China

⁵Institute Of High Energy Physics (IHEP), Beijing, China

⁶School of Physics State Key Laboratory of Nuclear Physics and Technology, Peking University, Beijing, China

⁷University of Chinese Academy of Sciences, Beijing, China

⁸Institute of Particle Physics, Central China Normal University, Wuhan, Hubei, China

⁹Consejo Nacional de Rectores (CONARE), San Jose, Costa Rica

¹⁰Université Savoie Mont Blanc, CNRS, IN2P3-LAPP, Annecy, France

¹¹Université Clermont Auvergne, CNRS/IN2P3, LPC, Clermont-Ferrand, France

¹²Aix Marseille Univ, CNRS/IN2P3, CPPM, Marseille, France

¹³Université Paris-Saclay, CNRS/IN2P3, IJCLab, Orsay, France

¹⁴Laboratoire Leprince-Ringuet, CNRS/IN2P3, Ecole Polytechnique, Institut Polytechnique de Paris, Palaiseau, France

¹⁵LPNHE, Sorbonne Université, Paris Diderot Sorbonne Paris Cité, CNRS/IN2P3, Paris, France

¹⁶I. Physikalisches Institut, RWTH Aachen University, Aachen, Germany

¹⁷Fakultät Physik, Technische Universität Dortmund, Dortmund, Germany

- ¹⁸*Max-Planck-Institut für Kernphysik (MPIK), Heidelberg, Germany*
- ¹⁹*Physikalisches Institut, Ruprecht-Karls-Universität Heidelberg, Heidelberg, Germany*
- ²⁰*School of Physics, University College Dublin, Dublin, Ireland*
- ²¹*INFN Sezione di Bari, Bari, Italy*
- ²²*INFN Sezione di Bologna, Bologna, Italy*
- ²³*INFN Sezione di Ferrara, Ferrara, Italy*
- ²⁴*INFN Sezione di Firenze, Firenze, Italy*
- ²⁵*INFN Laboratori Nazionali di Frascati, Frascati, Italy*
- ²⁶*INFN Sezione di Genova, Genova, Italy*
- ²⁷*INFN Sezione di Milano, Milano, Italy*
- ²⁸*INFN Sezione di Milano-Bicocca, Milano, Italy*
- ²⁹*INFN Sezione di Cagliari, Monserrato, Italy*
- ³⁰*Università degli Studi di Padova, Università e INFN, Padova, Padova, Italy*
- ³¹*INFN Sezione di Perugia, Perugia, Italy*
- ³²*INFN Sezione di Pisa, Pisa, Italy*
- ³³*INFN Sezione di Roma La Sapienza, Roma, Italy*
- ³⁴*INFN Sezione di Roma Tor Vergata, Roma, Italy*
- ³⁵*Nikhef National Institute for Subatomic Physics, Amsterdam, Netherlands*
- ³⁶*Nikhef National Institute for Subatomic Physics and VU University Amsterdam, Amsterdam, Netherlands*
- ³⁷*AGH - University of Science and Technology, Faculty of Physics and Applied Computer Science, Kraków, Poland*
- ³⁸*Henryk Niewodniczanski Institute of Nuclear Physics Polish Academy of Sciences, Kraków, Poland*
- ³⁹*National Center for Nuclear Research (NCBJ), Warsaw, Poland*
- ⁴⁰*Horia Hulubei National Institute of Physics and Nuclear Engineering, Bucharest-Magurele, Romania*
- ⁴¹*Affiliated with an institute covered by a cooperation agreement with CERN*
- ⁴²*DS4DS, La Salle, Universitat Ramon Llull, Barcelona, Spain*
- ⁴³*ICCUB, Universitat de Barcelona, Barcelona, Spain*
- ⁴⁴*Instituto Galego de Física de Altas Enerxías (IGFAE), Universidade de Santiago de Compostela, Santiago de Compostela, Spain*
- ⁴⁵*Instituto de Física Corpuscular, Centro Mixto Universidad de Valencia - CSIC, Valencia, Spain*
- ⁴⁶*European Organization for Nuclear Research (CERN), Geneva, Switzerland*
- ⁴⁷*Institute of Physics, Ecole Polytechnique Fédérale de Lausanne (EPFL), Lausanne, Switzerland*
- ⁴⁸*Physik-Institut, Universität Zürich, Zürich, Switzerland*
- ⁴⁹*NSC Kharkiv Institute of Physics and Technology (NSC KIPT), Kharkiv, Ukraine*
- ⁵⁰*Institute for Nuclear Research of the National Academy of Sciences (KINR), Kyiv, Ukraine*
- ⁵¹*University of Birmingham, Birmingham, United Kingdom*
- ⁵²*H.H. Wills Physics Laboratory, University of Bristol, Bristol, United Kingdom*
- ⁵³*Cavendish Laboratory, University of Cambridge, Cambridge, United Kingdom*
- ⁵⁴*Department of Physics, University of Warwick, Coventry, United Kingdom*
- ⁵⁵*STFC Rutherford Appleton Laboratory, Didcot, United Kingdom*
- ⁵⁶*School of Physics and Astronomy, University of Edinburgh, Edinburgh, United Kingdom*
- ⁵⁷*School of Physics and Astronomy, University of Glasgow, Glasgow, United Kingdom*
- ⁵⁸*Oliver Lodge Laboratory, University of Liverpool, Liverpool, United Kingdom*
- ⁵⁹*Imperial College London, London, United Kingdom*
- ⁶⁰*Department of Physics and Astronomy, University of Manchester, Manchester, United Kingdom*
- ⁶¹*Department of Physics, University of Oxford, Oxford, United Kingdom*
- ⁶²*Massachusetts Institute of Technology, Cambridge, Massachusetts, USA*
- ⁶³*University of Cincinnati, Cincinnati, Ohio, USA*
- ⁶⁴*University of Maryland, College Park, Maryland, USA*
- ⁶⁵*Los Alamos National Laboratory (LANL), Los Alamos, New Mexico, USA*
- ⁶⁶*Syracuse University, Syracuse, New York, USA*
- ⁶⁷*Pontificia Universidade Católica do Rio de Janeiro (PUC-Rio), Rio de Janeiro, Brazil
(associated with Universidade Federal do Rio de Janeiro (UFRJ), Rio de Janeiro, Brazil)*
- ⁶⁸*School of Physics and Electronics, Hunan University, Changsha City, China
(associated with Institute of Particle Physics, Central China Normal University, Wuhan, Hubei, China)*
- ⁶⁹*Guangdong Provincial Key Laboratory of Nuclear Science, Guangdong-Hong Kong Joint Laboratory of Quantum Matter,
Institute of Quantum Matter, South China Normal University, Guangzhou, China
(associated with Center for High Energy Physics, Tsinghua University, Beijing, China)*
- ⁷⁰*Lanzhou University, Lanzhou, China
(associated with Institute Of High Energy Physics (IHEP), Beijing, China)*
- ⁷¹*School of Physics and Technology, Wuhan University, Wuhan, China
(associated with Center for High Energy Physics, Tsinghua University, Beijing, China)*

⁷²*Departamento de Fisica, Universidad Nacional de Colombia, Bogota, Colombia
(associated with LPNHE, Sorbonne Université, Paris Diderot Sorbonne Paris Cité, CNRS/IN2P3, Paris, France)*

⁷³*Universität Bonn - Helmholtz-Institut für Strahlen und Kernphysik, Bonn, Germany
(associated with Physikalisches Institut, Ruprecht-Karls-Universität Heidelberg, Heidelberg, Germany)*

⁷⁴*Eotvos Lorand University, Budapest, Hungary
(associated with European Organization for Nuclear Research (CERN), Geneva, Switzerland)*

⁷⁵*Van Swinderen Institute, University of Groningen, Groningen, Netherlands
(associated with Nikhef National Institute for Subatomic Physics, Amsterdam, Netherlands)*

⁷⁶*Universiteit Maastricht, Maastricht, Netherlands
(associated with Nikhef National Institute for Subatomic Physics, Amsterdam, Netherlands)*

⁷⁷*Tadeusz Kosciuszko Cracow University of Technology, Cracow, Poland
(associated with Henryk Niewodniczanski Institute of Nuclear Physics Polish Academy of Sciences, Kraków, Poland)*

⁷⁸*Department of Physics and Astronomy, Uppsala University, Uppsala, Sweden
(associated with School of Physics and Astronomy, University of Glasgow, Glasgow, United Kingdom)*

⁷⁹*University of Michigan, Ann Arbor, Michigan, USA
(associated with Syracuse University, Syracuse, New York, USA)*
⁸⁰*Departement de Physique Nucleaire (SPhN), Gif-Sur-Yvette, France*

^aDeceased.

^bAlso at Università di Milano Bicocca, Milano, Italy.

^cAlso at Università di Roma Tor Vergata, Roma, Italy.

^dAlso at Università di Firenze, Firenze, Italy.

^eAlso at Scuola Normale Superiore, Pisa, Italy.

^fAlso at Università di Ferrara, Ferrara, Italy.

^gAlso at Università di Bologna, Bologna, Italy.

^hAlso at Università di Genova, Genova, Italy.

ⁱAlso at Università degli Studi di Milano, Milano, Italy.

^jAlso at Universidad de Coruña, Coruña, Spain.

^kAlso at Universidad Nacional Autónoma de Honduras, Tegucigalpa, Honduras.

^lAlso at Università di Cagliari, Cagliari, Italy.

^mAlso at Centro Federal de Educação Tecnológica Celso Suckow da Fonseca, Rio De Janeiro, Brazil.

ⁿAlso at Università di Bari, Bari, Italy.

^oAlso at Università di Perugia, Perugia, Italy.

^pAlso at LIP6, Sorbonne Université, Paris, France.

^qAlso at Universidade de Brasília, Brasília, Brazil.

^rAlso at Hangzhou Institute for Advanced Study, UCAS, Hangzhou, China.

^sAlso at Università di Pisa, Pisa, Italy.

^tAlso at Università di Padova, Padova, Italy.

^uAlso at Excellence Cluster ORIGINS, Munich, Germany.

^vAlso at Department of Physics/Division of Particle Physics, Lund, Sweden.

^wAlso at Università della Basilicata, Potenza, Italy.

^xAlso at Università di Siena, Siena, Italy.

^yAlso at Universidad de Alcalá, Alcalá de Henares, Spain.

^zAlso at Università di Urbino, Urbino, Italy.